Three-Point Synchrophasor Estimator With Better Off-Nominal Frequency Leakage Reduction

ROMAN NOVAK[ID], **(Member, IEEE)**

Department of Communication Systems, Jožef Stefan Institute, SI-1000 Ljubljana, Slovenia

e-mail: roman.novak@ijs.si

ABSTRACT Synchronous phasor measurements have long been an important tool in power flow modelling and network state estimation as well as in many other tasks that support power grid observability. Classic phasor estimation algorithms are often preferred over complex alternatives. They are based on a variant of the Discrete Fourier Transform (DFT) while relying on a sampling frequency locked to the system nominal frequency. The spectral leakage caused by the small off-nominal frequency excursions in such settings introduces errors that are handled by the estimation algorithms to a different extent. Well-known three-point averaging filter (3P) is a low-cost spectral leakage reduction technique in one of the simplest estimators based on a single-bin DFT. However, it only partially removes the oscillating components. When an independent standard-based frequency tracking is available, the errors can be further compensated with minimal cost. We propose a frequency-corrected three-point estimator (F3P) to eliminate the induced spurious spectrum progressively with the increasing sampling rate while building on the analytical expression of the remaining error. We show performance benefits of the F3P under finite sampling rates when compared to the baseline 3P and to the classical Interpolated DFT (IPDFT) in static conditions. The F3P removes most of the leakage without the need of data resampling. In less ideal conditions with additive 50-dB noise, up to a 10-fold reduction of the 3P error is achieved. The error ratio of the reference IPDFT over the F3P is approximately 1.4 under the same conditions and largely independent of the frequency excursion. The presented simulation results prove the algorithm's superior performance in most of the steady-state tests defined by the relevant Standard, whereas the dynamic performance can be brought to an acceptable level by the use of a single-cycle observation window, with the response times comparable to those of the IPDFT.

INDEX TERMS Digital signal processing, discrete Fourier transform, measurement errors, phasor measurement unit, power distribution, synchrophasor.

I. INTRODUCTION

Power grid observability is based on the increasingly sophisticated measurement instruments and techniques. Voltage or current phasor representation, i.e., magnitude and phase angle at a selected measurement point, is the key parameter, among many other uses, for modelling power flow, network state estimation, wide are control, or for critical event detection. Phasor Measurement Units (PMUs) are commonly deployed over the transmission networks. They are gradually installed in the distribution grids as well [1], where the more dynamic operational parameters raise stringent accuracy requirements. For instance, lower power flows and shorter line distances are just two reasons for the reduced phase displacement of the synchronous measurements. Low voltage differences also constrain the tolerable error levels of the synchronous measurements, with the misalignment of the external clock references further penalizing the measurement accuracy. The latter is also caused by the use of diverse clock synchronization techniques.

Phasor estimation algorithm is at the core of PMU-like devices. In order to estimate a phasor from the set of acquired samples, the algorithm typically adopts a form of Discrete Fourier Transform (DFT), modifying it in a way to derive properties of a single fundamental frequency. Because the actual frequency of power systems dynamically fluctuates within a relatively narrow range, data sampling is commonly locked to the system's rated frequency provided by

---

The associate editor coordinating the review of this manuscript and approving it for publication was Li Zhang.

an external clock reference. Other approaches are certainly possible; however, they typically increase the complexity of measurement devices.

The fact that sampling process is slightly out of sync from the actual off-nominal frequency leads to the well-known spectral leakage in the DFT [2]. The leakage shows as the induced spurious spectrum due to discontinuities at the sample window boundaries. It is a primary source of errors in the estimated phasors. In addition to the underestimated magnitudes and shifted angles, a stream of consequent estimates exhibits slow and fast oscillations both in magnitude and phase angle, with the severity depending on the difference between the nominal and the actual frequency. The oscillations, especially the faster ones, are a cause of concern because they affect the comparison of imprecisely synchronized measurements and even more those following in time. Note that in power systems we are mostly concerned with the difference of two phasors. As demonstrated latter, the fast oscillations occur at the second harmonic of the measured off-nominal frequency if the above estimation principle is used.

Although some of the effects of frequency leakage can be considerably minimized by adopting an appropriate window function, a three-point averaging filter (3P) proves to be very effective while using the simplest rectangular window and a single-bin DFT [3]. However, the second-harmonic ripple is not entirely eliminated and some error remains. The objective of the presented work is to eliminate this type of error further in order to improve the estimation accuracy even with the loosely synchronized clocks while preserving fast response and low complexity of the baseline algorithm. We focus on the estimators with good performance under the static conditions, as required by many power grid applications. In accordance with the distinction made by the recently published International Standard that regulates synchrophasor measurement devices for power systems IEC/IEEE 60255-118-1 [4], i.e., the Standard, those estimators are better suited for the measurement M-class devices as opposed to the protective P-class devices.

In summary, the contributions of this paper are as follows.

- Frequency-corrected three-point averaging filter (F3P) is proposed to efficiently remove most of the off-nominal frequency leakage in the subsequently evaluated magnitudes and phase angles under the steady-state conditions.
- An independent Standard-complying frequency tracker is only employed to preserve the low computational cost and the responsiveness of the baseline estimator.
- No amplitude or phase angle calibration is required due to the frequency-mismatched data sampling. An additional reduction of the discretization error and, hence, the faster convergence towards the total elimination of the leakage-induced effects is achieved by the intra-sample phasor interpolation.
- The F3P is being shown to outperform the reference Interpolated DFT (IPDFT) [5], [6] in most of the

steady-state tests defined by the Standard. In addition, the impact of sampling rate on the F3P performance has been studied. One-cycle variant of the F3P is proposed in order to improve the dynamic performance.

In the following, a brief survey of related work is presented in Section II. In Section III we recall the analytical expression for the leakage if single-bin DFT is estimated at off-nominal frequency while using rated frequency clock. Next, the remaining error after the three-point average is derived. Frequency-corrected filtering is then showed to eliminate the second harmonic ripple in settings with no discretization error. Phasor interpolation is introduced as a way to reduce that discretization error below sampling rate limits. The F3P is evaluated in Section IV, where a comparison is made with the classical IPDFT. The analysis is focused on the standardized steady- and dynamic-state tests. Further, we quantify the impact of the sampling frequency and provide a comparison of the estimator to some of the state-of-the-art proposals. A short discussion is given in Section V, followed by the conclusion in Section VI.

II. RELATED WORK
The research of phasor estimation algorithms is generally driven by the three main factors, namely the efficiency of handling the off-nominal frequencies, the overall accuracy and the tradeoff between the accuracy and the responsiveness. Variations of the discrete Fourier technique are the most common [7]–[9], with Kalman filter [10] and the least-squares methods [11], [12] as the more complex options for improving the accuracy while sacrificing the simplicity. Note that the proposed F3P belongs to the first DFT-based group. Frequency tracking and resampling is another technique to reduce the errors [3]. The estimators that completely abandon the DFT approach find their foundation in a complex Taylor expansion [13], wavelets [14], adaptive filtering [15] or in the signal subspace [16]. The flat-top finite-impulse response filters can efficiently handle harmonic phasor estimation while using a bank of quadrature oscillators [17]. On the other hand, maintaining a fast response time while providing acceptable accuracy is best captured by the IPDFT [18] and some of its improvements [5], [6], [19], [20], although the fast response times of the latter are questionable. Iterative approaches are commonly used to improve accuracy in the off-nominal case [21]. Other calibration-based methods have been proposed that take into account a power system model to eliminate erroneous phase angle differences [22]. The impact of measurement errors on the synchrophasor-based applications is also widely studied, with a more recent systematic evaluation in [23]. Table 1 presents some highlights and limits of the aforementioned phasor estimation techniques.

III. CORRECTION OF THE LEAKAGE EFFECT
The leakage phenomenon represents the dominant source of errors if phasor estimate is based on the discrete Fourier transform. In order to quantify that error, let us first assume

TABLE 1. Phasor estimation techniques.

Underlying principle	References	Highlights	Limits
Pure DFT	[3], [7]–[9]	Simple and well understood	Steady-state conditions preferred Off-nominal frequency leakage (reduced in F3P)
Interpolated DFT	[5], [6], [18]–[20]	Different window functions and window lengths for application-specific behavior	Complex Remaining off-nominal frequency leakage Poor out-of-band interharmonics performance
Kalman filter	[10]	Estimate using small number of samples	Nonlinear filters have stability problems
Least squares optimization	[11], [12]	Low noise sensitivity Recursive and non-recursive forms	Poor performance in the presence of harmonics
Resampling	[3]	Avoids off-nominal frequency leakage	Requires good frequency estimate Sample interpolation introduces errors
Taylor expansion	[13]	Designed for dynamic conditions Allows estimation of higher order derivatives	Best for protection and control devices
Wavelets	[14]	Supports half data cycle windows	Less accurate in dynamic conditions even when compared to DFT
Adaptive filtering	[15]	Flexible under oscillation conditions Provides estimates of first derivatives	Intended for protection applications
Signal subspace	[16]	Designed for dynamic conditions	High sampling rate required Resource-demanding implementation
Flat-top FIR filters	[17]	Simultaneous estimation of multiple harmonics	Oversized for the fundamental frequency Measurement applications only
Calibration based	[22]	Accurate correction of phase angle	Static conditions and post processing required Restricted to line parameters estimation

that the signal can be modelled by a sinusoid

$$x(t) = X_m \cos(2\pi f t + \phi) \qquad (1)$$

with a frequency f, phase shift ϕ and peak amplitude X_m. A complex number

$$X = \frac{X_m}{\sqrt{2}} e^{j\phi} \qquad (2)$$

is then, by definition, the phasor representation of (1). In power systems the root mean square (RMS) value of the input signal is more customary than the peak amplitude, hence the division of X_m by $\sqrt{2}$. Measuring equipment makes use of a digitized stream $x_n = x(n\Delta t)$ at fixed sampling rate $F_s = 1/\Delta t$. A multiple of the system nominal frequency Nf_0 is commonly chosen as the sampling frequency in phasor measurement devices [3], [5]. Given an interval of M sampling points, where M is an integer multiple of N, i.e., $M = pN, p \in \mathbb{N}_1$, the most straightforward way of estimating (2) under the above conditions is to compute the p-th harmonic component of the normalized DFT

$$X'_r = \frac{\sqrt{2}}{M} \sum_{n=r}^{r+M-1} x_n e^{-\frac{j2\pi pn}{M}}, \qquad (3)$$

where the use of running index r eliminates phase rotation due to the computation shift. Under the assumption of noise-free $x(t)$ and infinite computing precision, (2) is exactly equal to (3) if $f = f_0$ and $N > 2$. If f is only close to f_0, as it is the case in power systems, (3) is an approximation of (2) due to the well-known DFT leakage phenomenon. The exact relation between the two expressions in closed form for a given discretization index r is derived in [3] and can

be written as

$$X'_r = PX e^{jr(\omega-\omega_0)\Delta t} + QX^* e^{-jr(\omega+\omega_0)\Delta t}$$

$$P = \frac{\sin \frac{M(\omega-\omega_0)\Delta t}{2}}{M \sin \frac{(\omega-\omega_0)\Delta t}{2}} e^{j(M-1)\frac{(\omega-\omega_0)\Delta t}{2}},$$

$$Q = \frac{\sin \frac{M(\omega+\omega_0)\Delta t}{2}}{M \sin \frac{(\omega+\omega_0)\Delta t}{2}} e^{-j(M-1)\frac{(\omega+\omega_0)\Delta t}{2}} \qquad (4)$$

where $\omega = 2\pi f$, $\omega_0 = 2\pi f_0$ and X^* is a complex conjugate of the true phasor representation X. In other words, X'_r is the calculated phasor representation of a noise-free $x(t)$ if a single-bin DFT without any elaborate windowing, i.e., rectangular window, is taken at nominal frequency f_0. The two summation terms in (4) consist of complex attenuation parts PX and QX^*, which are independent of discretization index r and rotate at angular speeds of $\omega - \omega_0$ and $\omega + \omega_0$, respectively. The two rotations show as a composite magnitude oscillation at the angular frequency of 2ω. Also due to the compound effect of both rotations, the phase angle falsely drifts and oscillates as illustrated in Fig. 1.

The faster oscillations can have severe consequences for a comparison of slightly misaligned measurements or for the applications where precise phasor value is required, and they should preferably be removed. On the other hand, the slower phase drift, which is also an oscillation in longer term, is much less disturbing and is tolerated even in the state estimators [24]. Moreover, the latest Standard requires this type of phasor rotation to be included in the reported phasors if the power system frequency is different from its nominal value. Note, however, that factor P should still be eliminated by the phasor estimation algorithm.
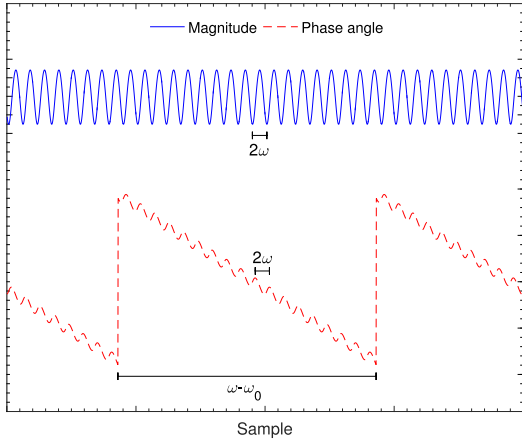
FIGURE 1. Illustration of an exaggerated DFT leakage effect on the estimated magnitude and phase angle.

FIGURE 2. Additional attenuation factors introduced by 3P to the closed-form expression.

A three-point averaging filter (3P) has been regularly used to mitigate the faster oscillations before the appearance of more elaborate estimators [3]. The filter averages three phasor estimates spaced at constant phase angle of $\pi/3$ with respect to the nominal frequency. This corresponds to the angle difference of $2\pi/3$ for the second harmonic. The 3P can be written as

$$X_r^{3P} = \frac{1}{3}(X'_{r-\frac{N}{6}} + X'_r + X'_{r+\frac{N}{6}}). \quad (5)$$

In discrete units the spacing angle equals $N/6$ samples. Apart from the frequency dependent attenuation compensation due to the already mentioned P and Q terms, the correction of the estimator oscillations has, to the best of our knowledge, stopped here. The assumption has been that the remaining error is negligible for practical applications, arguing that $\Delta\omega = \omega - \omega_0$ is sufficiently small in power systems, whereas $\omega + \omega_0$ is close enough to $2\omega_0$ for which the three-point average works perfectly. We show that an order of magnitude more precise phasor estimate can be achieved by going one step further, which in steady-state conditions brings largely inferior 3P estimator on par with or better than more complex state-of-the-art estimators.

First, by using identities $r\Delta t = t$, $N\Delta t = T_0$ and $T_0 = 2\pi/\omega_0$, one can estimate a closed-form alternative to (4) for a DFT with the addition of the three-point average as

$$X_r^{3P} = PXe^{jr(\omega-\omega_0)\Delta t}\left(\frac{1}{3} + \frac{2}{3}\cos\left((1-\frac{\omega}{\omega_0})\frac{\pi}{3}\right)\right)$$
$$+ QX^*e^{-jr(\omega+\omega_0)\Delta t}\left(\frac{1}{3} + \frac{2}{3}\cos\left((1+\frac{\omega}{\omega_0})\frac{\pi}{3}\right)\right).$$
$$(6)$$

The derivation of (6) is provided in Appendix A. The three-point average only attenuates the original summation terms. Fig. 2 shows the actual attenuation factors for the off-nominal frequencies in the range of ± 5 Hz, which fits the widest frequency range of the standard M-class compliance. At both
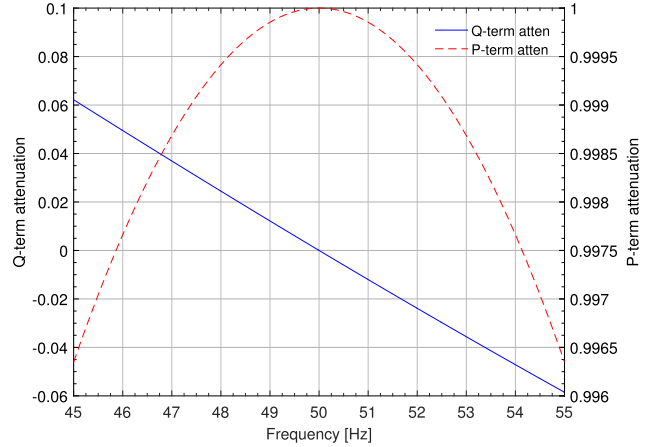
frequency extremes, Q-term, which is responsible for the faster oscillations, still keeps up to 6% of its unfiltered value.

Here, a modified three-point average is proposed with the spacing corrected by factor

$$k = \frac{2\omega_0}{\omega + \omega_0}. \quad (7)$$

The redefined frequency-corrected three-point average

$$X_r^{F3P} = \frac{1}{3}(X'_{r-k\frac{N}{6}} + X'_r + X'_{r+k\frac{N}{6}}), \quad (8)$$

using the same substitutions as in derivation of (6), entirely eliminates the second term in the closed-form expression

$$X_r^{F3P} = PXe^{jr(\omega-\omega_0)\Delta t}\left(\frac{1}{3} + \frac{2}{3}\cos\left(\frac{2\pi}{3}\frac{(\omega-\omega_0)}{(\omega+\omega_0)}\right)\right). \quad (9)$$

The derivation of (9) is provided in Appendix B. Because $kN/6$ is generally a real number, it needs to be rounded to the closest integer. Therefore (8) only converges to the closed-form expression as the sampling rate tends to infinity. The slowly rotating phasor is finally acquired by dividing (9) with the remaining complex attenuation constant.

Correction factor k establishes the ideal three-point spacing for the elimination of the Q-term due to

$$(\omega + \omega_0)k\frac{T_0}{6} = \frac{2\pi}{3}. \quad (10)$$

In practice, such an ideal cancellation cannot be achieved for at least two reasons. The actual frequency can only be estimated and there is no such thing as an infinite sampling rate.

Finite sampling rate inevitably introduces errors. While N can be chosen such that $N/6$ is integer value, $kN/6$ is generally noninteger value. Discretization artefacts at given sampling rate can be reduced by using interpolation between the known discrete-time values. Here, a linear interpolation is proposed because of its low-cost implementation and good

performance. For instance, the interpolation of the first summation term in (8) can be done as

$$X'_{r-k\frac{N}{6}} \approx X'_{r_L} + \mu(X'_{r_H} - X'_{r_L}), \qquad (11)$$

where $r_L = \lfloor r - kN/6 \rfloor$ and $r_H = \lceil r - kN/6 \rceil$ are the lower and upper integer indices, respectively, whereas $\mu = r - kN/6 - r_L$ is the interpolation factor.

The F3P requires an estimate of the actual frequency, which is not calculated by the algorithm itself, like, for example, by the six-parameter, second order Taylor's expansion [13]. Here we rely on the existing frequency tracking algorithms. In order to maintain the independence of the phasor estimation algorithm from the actual frequency tracker, we distance ourselves from the particular implementation, but assume that frequency estimation is compliant with the Standard in terms of the maximum frequency error (FE) allowed for a specific operational condition. The interested reader is referred to [3] for a comprehensive introduction on the frequency estimation techniques.

IV. EVALUATION

We assess the accuracy of the F3P with respect to the static and dynamic performance metrics outlined in the synchrophasor measurements standard [4]. The evaluation is not a measurement compliance test as that would require actual laboratory tests of physical PMU device as a whole, which includes the influence of other functional blocks, such as analogue front end and filtering. Nevertheless, we test the core algorithm in isolation and compare the results to those provided in [5], where similar methodology was used to evaluate and compare the IPDFT to the number of alternatives. In that way, a comparison is established between multiple synchrophasor evaluation algorithms without the need to actually implement all of them. The steady-state tests include off-nominal frequency offset test, accuracy assessment in the presence of additive wideband noise, as well as harmonics and out-of-band interference tests. On the other hand, the dynamic performance tests assess the accuracy of phasor estimates of a modulated signal, measure performance during a system frequency ramp, and evaluate phasors during abrupt steps in amplitude or phase angle. The performance measure used in the evaluation is the Total Vector Error (TVE), which is the normalized difference between the reference and the assessed phasor, sensitive to both the amplitude and the phase angle error

$$\text{TVE} = \frac{|X' - X_{\text{ref}}|}{|X_{\text{ref}}|}. \qquad (12)$$

The maximum frequency errors considered are those specified by the Standard for the more limiting P-class devices. In the steady-state tests $\pm 0.005\,\text{Hz}$ is assumed, whereas under the dynamic conditions $\pm 0.06\,\text{Hz}$, $\pm 0.01\,\text{Hz}$ and $\pm 0.005\,\text{Hz}$ maximum FEs are applied in the modulation, ramp and step tests, respectively.

A. REFERENCE IPDFT ESTIMATOR

We take the IPDFT as a reference approach in the following analysis. The IPDFT variants are among the most frequently used algorithms in synchrophasor measurements with good performance in terms of residual error. The base principles and formulas are given next for the sake of completeness. Further theoretical and practical details are available in several texts, e.g., [5], [6], [18], [20]. We choose the algorithm variant with the best documented performance [5], [6].

Although not strictly needed, the assumption of the off-nominal frequency deviating from the nominal frequency less than half of the DFT frequency resolution δ_f simplifies both the formulation and the algorithm implementation

$$|f - f_0| \leq \frac{\delta_f}{2}, \qquad (13)$$

where δ_f equals F_s/M with F_s being the sampling rate and M the window length. In the first step, the selected IPDFT applies a maximum sidelobe decay (MSD) window to the input signal and computes the DFT

$$Y(k) = \sum_{m=0}^{M-1} w_m x_m e^{-\frac{jk2\pi m}{M}} \quad k \in [0 \ldots M-1], \qquad (14)$$

where the H-term MSD belongs to the cosine windows with the most rapidly decaying sidelobes [6]

$$w_m = \sum_{h=0}^{H-1} (-1)^h a_h \cos \frac{2\pi hm}{M} \quad m \in [0 \ldots M-1]. \qquad (15)$$

The number of samples M is required to span several cycles of the nominal frequency, typically 2 to 5. In the case of $H = 3$, the window coefficients are $a_0 = 0.375$, $a_1 = 0.5$ and $a_2 = 0.125$. Note that F3P parameter p is equivalent to H. We keep the original notation of IPDFT for clarity.

Let the location of the DFT maximum of (1) is at fixed index k_{max}. In the next step, the IPDFT chooses the second largest DFT amplitude either at $k_{\text{max}} - 1$ or $k_{\text{max}} + 1$ and sets parameter ε to 0 or 1, respectively. This step prevents using a single cycle M because k_{max} must be at least 2. In order to compute phasor representation of the input signal, α and δ_{bin} are calculated next as

$$\alpha = \frac{|Y(k_{\text{max}} + \varepsilon)|}{|Y(k_{\text{max}} - 1 + \varepsilon)|} \qquad (16)$$

$$\delta_{\text{bin}} = \frac{(H - 1 + \varepsilon)\alpha - H + \varepsilon}{\alpha + 1}. \qquad (17)$$

The final interpolation step gives an estimate in the form of peak amplitude Y_m and phase angle ϕ

$$Y_m = \frac{2^{2H-1}\pi \delta_{\text{bin}} |Y(k_{\text{max}})|}{M \sin(\pi \delta_{\text{bin}})(2H-2)!} \prod_{h=1}^{H-1} (h^2 - \delta_{\text{bin}}^2) \qquad (18)$$
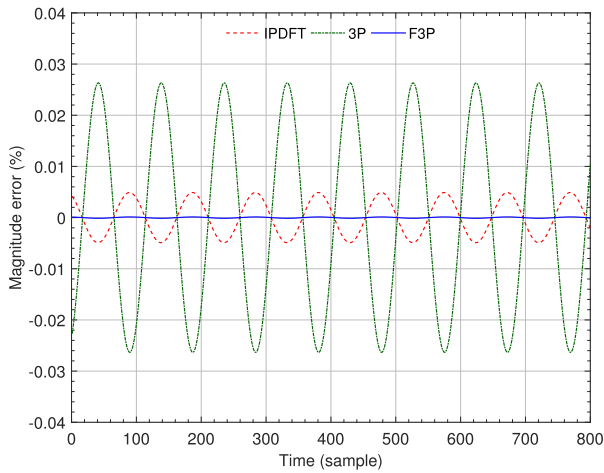
$$\phi = \angle Y(k_{\text{max}}) - \pi \delta_{\text{bin}} + \pi \frac{\delta_{\text{bin}}}{M} - \frac{\pi}{2} \text{sign}(\delta_{\text{bin}}) - \angle W - \frac{\pi}{2}, \qquad (19)$$

where

$$W = \sum_{h=0}^{H-1}(-1)^h 0.5 a_h$$
$$\left[\frac{e^{-\frac{j\pi h}{M}}}{\sin(\frac{\pi}{M}(-\delta_{bin} - h))} + \frac{e^{\frac{j\pi h}{M}}}{\sin(\frac{\pi}{M}(-\delta_{bin} + h))} \right]. \quad (20)$$

B. STEADY-STATE EVALUATION

Steady-state tests are designed to measure phasor accuracy in conditions under which the amplitude, frequency and phase angle are fixed for the period of the measurement.

FIGURE 3. 3-cycle IPDFT [5] (red), 3P [3] (green) and F3P (blue) magnitude oscillations at $f = 51.5$ Hz, $F_S = 10000$ samples/second and $f_0 = 50$ Hz; the estimators are applied to a noise-free signal.
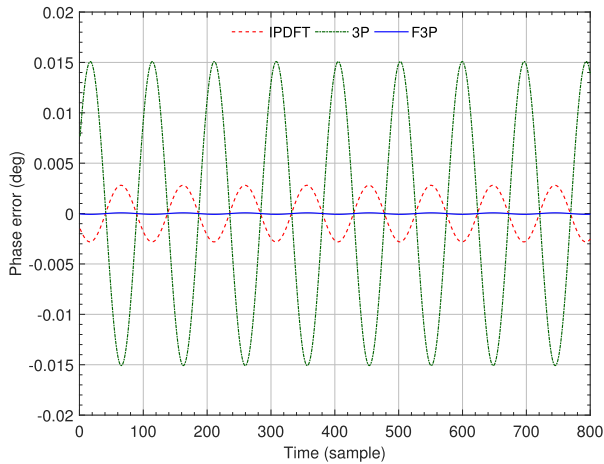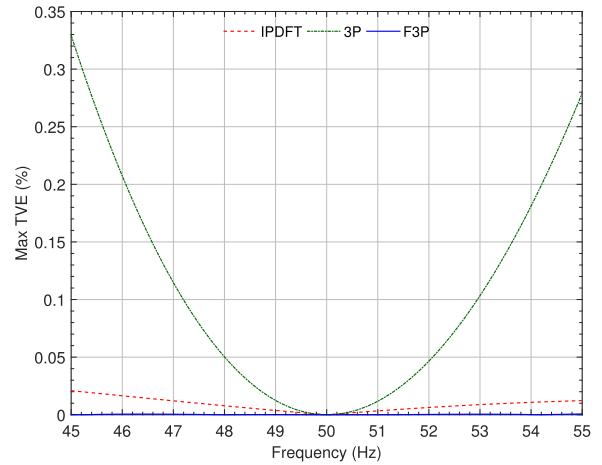

FIGURE 4. 3-cycle IPDFT [5] (red), 3P [3] (green) and F3P (blue) phasor angle oscillations at $f = 51.5$ Hz, $F_S = 10000$ samples/second and $f_0 = 50$ Hz when applied to a noise-free sinusoid.

1) OFF-NOMINAL FREQUENCY OFFSET TEST

The off-nominal frequency offset test, in particular, is the fundamental steady-state test to measure the amount of remaining spectral leakage due to mismatched sampling rate. According to the Standard, maximum TVE must be observed over the full test interval. The importance of the maximum value is illustrated in Fig. 3 and Fig. 4, where the magnitude

and phase errors are shown for consequent discretization indices. The 3-cycle IPDFT is compared to the 3-cycle 3P and F3P. The number of samples per rated 50 Hz cycle was set to 200, i.e., $F_s = 10000$. The remaining fast oscillation for a chosen off-nominal frequency of 51.5 Hz is significant for the 3P and less pronounced for the IPDFT. In the case of F3P, the oscillation is barely noticeable, but still present due to the finite sampling rate.

FIGURE 5. Maximum TVE of estimated phasors of a noise-free sinusoid in the range of ±5 Hz from the nominal 50 Hz are shown for the 3-cycle IPDFT [5] (red), 3P [3] (green) and F3P (blue) at $F_S = 10000$ samples/second.

The maximum TVE for a selected range of off-nominal frequencies is depicted in Fig. 5 for a 10-second stream. Because most power systems operate in a relatively narrow band of frequency, the off-nominal frequency range of 50 Hz ± 5 Hz is considered sufficiently wide for the analysis. The range is also recommended for the M-class compliance in the Standard, whereas P-class devices targeting fast response protection applications have narrower frequency range requirements. In Fig. 5, the algorithm parameters are set to $N = 200$, $p = H = 3$ and $f_0 = 50$ Hz. Overall, the F3P manages to reduce the maximum TVE for at least an order of magnitude in comparison to the 3P and the IPDFT over the entire frequency range. In the case of IPDFT, most of the error is caused by the spectral interference from the image component [5]. On the other hand, the remaining F3P error is strictly a consequence of the finite sampling rate.

Under the noise-free steady-state conditions and in line with (8), the F3P should eliminate fast oscillations in phasor estimates when sampling rate approaches infinity. Next, we want to establish the amount of residual TVE under the realistic finite sampling rates. For comparison purposes, the input signal is still assumed to be noise-free and without measurement inaccuracies. Fig. 6 shows the maximum TVE as a function of the number of samples per nominal cycle for sampling rates from 1 to 20 kHz. Again, the off-nominal frequency of 51.5 Hz is selected to demonstrate the differences between the three estimators.
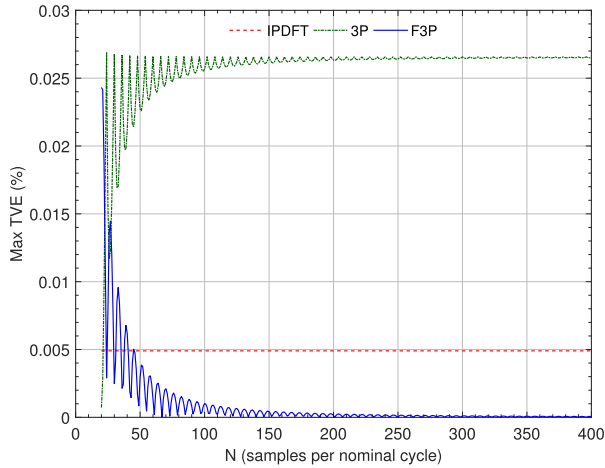
FIGURE 6. The impact of finite sampling rates on the maximum TVE; shown are 3-cycle IPDFT [5] (red), 3P [3] (green) and F3P (blue) estimates at $f = 51.5\,\text{Hz}$.
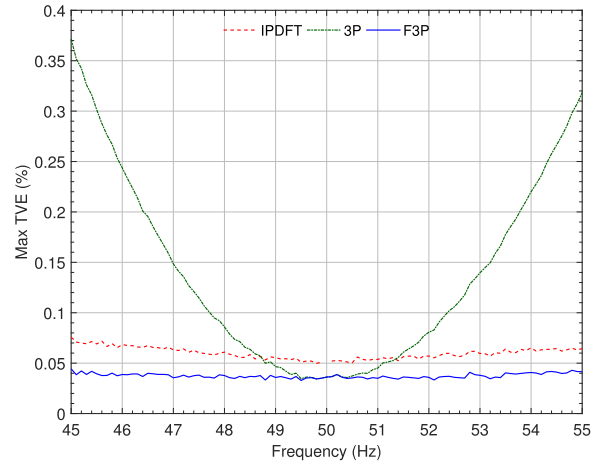

FIGURE 7. Performance of 3-cycle F3P (blue) versus IPDFT [5] (red) and 3P [3] (green) estimators; white Gaussian noise is added to the input sinusoid at 50 dB SNR and $F_S = 10000$ samples/second.

With respect to the 3P estimator, the maximum TVE converges towards the theoretical value that follows from (6). As expected, the F3P TVE quickly approaches zero with less accurate interpolation lobes and minimums at values for which $kN/6$ is being close to integer. On the other hand, the IPDFT is not sensitive to the sampling rate. However, its constant maximum TVE is quickly outperformed by the 3FP, e.g., in Fig. 6 for the sampling rates over 2.5 kHz. Because sampling rate must be chosen sufficiently high to avoid the aliasing effects on the input signal, this should not be a problem for real devices. In conclusion, the F3P presents attractive properties. It exhibits a monotonically decreasing error and the off-nominal frequency independence. Further, all estimators are well below the 1% TVE threshold recommended by the Standard.

2) ADDITIVE WIDEBAND NOISE TEST

Phasor estimation takes place in practice on a noisy input. Measurement errors alone can be regarded as a noise, though high-frequency transients and harmonics of the prevailing system frequency are far larger contributors. Uncertainties can be further attributed to the synchronization mechanisms, data acquisition equipment and to the transducers. Here we deal with the additive wideband noise, for which a separate test is defined by the Standard. Some of the disruptions are evaluated by the dynamic-state tests later on, whereas harmonics are targeted in the next subsection.

The other parameters being fixed as in the off-nominal frequency offset test, we introduce a zero-mean, normally distributed additive white Gaussian noise with variance corresponding to the 50 dB signal-to-noise ratio (SNR). The results are presented in Fig. 7.

The 3-cycle F3P performs better than both reference estimators under the same simulation conditions even though the IPDFT handles abrupt changes in the extracted portion of a signal with a smooth window function, tailing off signal

more gradually as the F3P square windowing. However, the approximations made by other parts of the IPDFT algorithm cancel this advantage. All results in Fig. 7 are below the 1% TVE threshold. Note that the error of a frequency tracker is also negligible for the first two steady-state tests. Indeed, the frequency estimation proposed in [3] and amended with a single-cycle averaging filter is highly efficient in such conditions. The FE can easily be reduced well below the required ± 0.005 Hz.
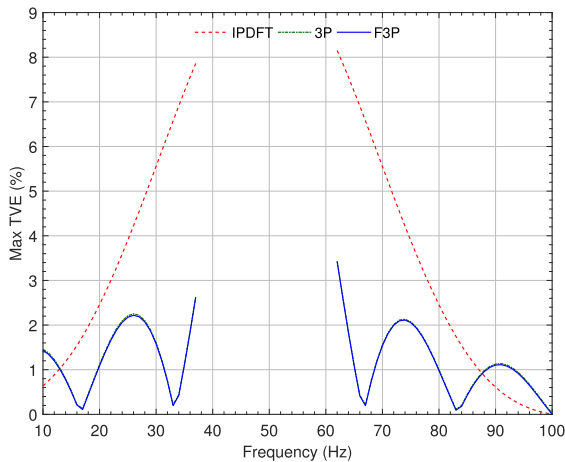
3) HARMONIC DISTORTION

Input signals may be corrupted by the harmonics. The actual impact on the estimator's accuracy decreases with the harmonic number. Therefore, only the second harmonic test is presented here, for which the maximum distortion is expected. Further, 10% of the fundamental amplitude is used for the interfering harmonic signal, which is the larger of the two values in [4]. With respect to the above conditions, this is the first test, where the IPDFT surpasses the F3P in terms of the evaluated fundamental phasor accuracy, as shown in Fig. 8. In order to reduce the error below the 1% TVE threshold, an additional correction is necessary, such as to evaluate the second harmonic phasor first and subtract the value from the estimated fundamental phasor. Similar approach can be found in [5]. Applying the FE of ± 0.005 Hz in this test leads to 0.1 increase of the maximum TVE.

4) OUT-OF-BAND INTERFERENCE

The quality of a phasor estimation algorithm is evaluated next in terms of its filtering capability of interfering frequencies that fall outside the power system operating range, i.e., out-of-band frequencies. According to the Standard, the minimum interfering frequency range should span from 10 to 100 Hz for the nominal frequency of 50 Hz. Further, the passband is coupled to the phasor reporting rate. In the case of 25 reports per second, the excluded passband evaluates
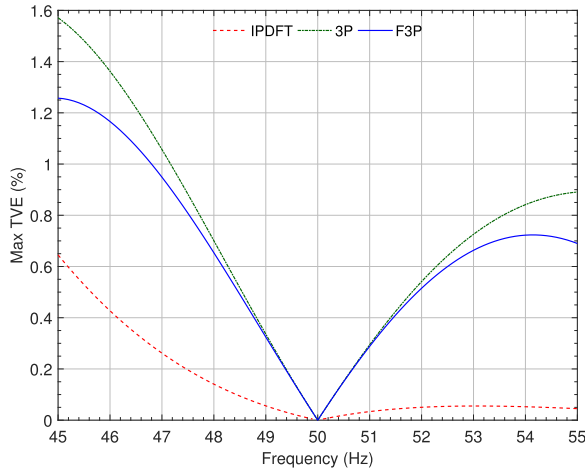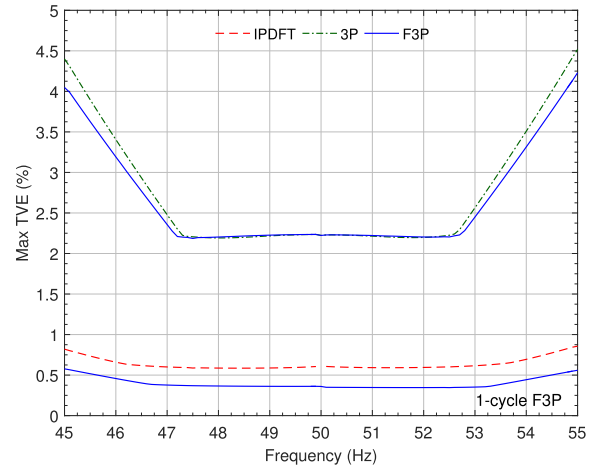
FIGURE 8. Second-harmonic distortion test for 10% harmonic amplitude and 3-cycle IPDFT [5] (red), 3P [3] (green) and F3P (blue) estimators at $F_s = 10000$ samples/second.

FIGURE 9. Out-of-band interference rejection test in the range from 10 to 100 Hz, excluding the passband; 3-cycle IPDFT [5] (red), 3P [3] (green) and F3P (blue) estimators are applied to the fundamental power signal at $f = 48.75$ Hz, which is interfered with sinusoids at 10% of the fundamental magnitude level.

FIGURE 10. Maximum TVE of modulated off-nominal frequency; 1- and 3-cycle F3P (blue) is compared to the 3-cycle IPDFT [5] (red) and 3P [3] (green) using both the amplitude and the phase angle modulation factor of 0.1 and 5 Hz modulation frequency.

C. DYNAMIC PERFORMANCE

The proposed estimator is based on the intrinsically static phasor model, derived under the assumption of a steady-state sinusoidal waveform in accurate measurement applications. Nonetheless, we also give the results of the three standardized tests to evaluate the expected dynamic performance.
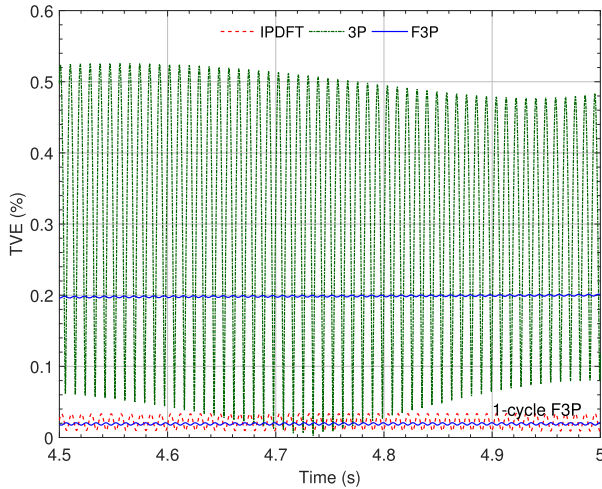
1) MODULATION TEST

The modulation test is designed to establish the minimum synchrophasor measurement bandwidth. For that purpose, the input needs to be modulated in amplitude and/or phase. The phasor measurement should be within the 3% TVE limit at the nominal frequency. Because Fig. 10 gives a maximum TVE for the whole range of off-nominal frequencies, only central values are subject to the limit. Presented is the worst case when both the amplitude and the phase angle modulation are applied at the same time while using 0.1 for the modulation factors and the modulation frequency of 5 Hz. The 3-cycle F3P is clearly outperformed by the IPDFT, but still under the 3% TVE limit. On the other hand, the 1-cycle F3P takes advantage of a shorter observation window and reduces the error the most. The use of maximum FE of ± 0.06 Hz affects mostly the frequencies at both ends of the presented range with the flat region remaining closely to that of Fig. 10.

2) FREQUENCY RAMP TEST

Performance during a linear ramp of the system frequency is the second dynamic test. In Fig. 11, a constant ramp rate R_f of 1 Hz/s is applied to the nominal frequency from the start. The measured TVE in the interval between 4.5 and 5 seconds is shown for the three 3-cycle estimators as well as for the 1-cycle F3P. While the 3P shows a periodic envelope, the IPDFT and F3P steadily increase the TVE with the slope barely noticeable. The IPDFT surpasses the 3-cycle F3P in

at $[f_0 - 25/20, f_0 + 25/20] = [37.5, 62.5]$ Hz. Off-nominal frequency $f = 48.75$ Hz is chosen in the tests presented in Fig. 9. The required magnitude level of the interfering signals, introduced one at a time, is 10% of the measured sinusoid magnitude.

The F3P has better out-of-band interharmonic rejection capability than the IPDFT for most of the observed range. The exception are frequencies below 13 Hz and above 88 Hz. However, the 1.3% TVE threshold is only reached for roughly half of the tested out-of-band frequencies. Better performance would require an additional filtering of the input signal. Similar to the previous test, 0.1 increase of the maximum TVE is observed if the FE is set to ± 0.005 Hz.

FIGURE 11. Frequency ramp test; time snapshot of the TVE is shown for the 1-cycle F3P (blue and labeled) and 3-cycle IPDFT [5] (red), 3P [3] (green) and F3P (blue) estimators at 1 Hz/s linear ramp rate, when applied to the nominal frequency from time zero.

FIGURE 12. Amplitude step test; a 10% step in amplitude is applied to a sinusoid at nominal frequency. The plotted TVE of the 1-cycle F3P (blue and labeled) and 3-cycle IPDFT [5] (red), 3P [3] (green) and F3P (blue) estimators show their dynamic behavior around the transition time.
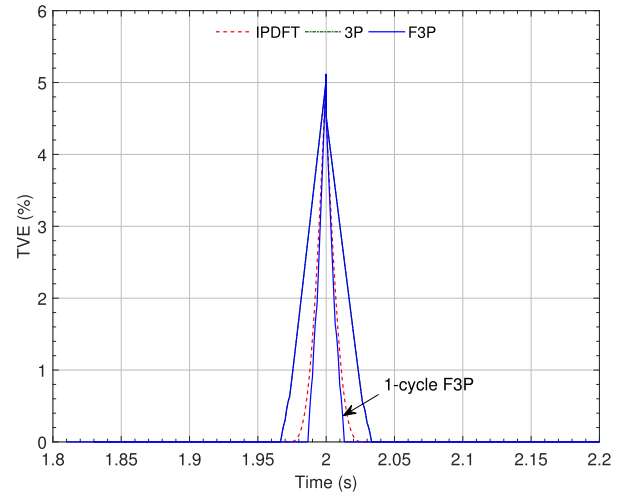
terms of accuracy. Similar conclusion does not hold when the IPDFT is compared to the 1-cycle F3P, with the F3P showing better performance. Note that if the frequency tracker is allowed to fluctuate randomly with the maximum FE of ± 0.01 Hz, which is the value permissible by the Standard for the reference frequency

$$f(t) = f_0 + R_f t, \tag{21}$$

the TVE increases to 0.08% and 0.39% for the 1- and 3-cycle F3P, respectively. However, all the estimators are within the 1% TVE threshold.

3) AMPLITUDE AND PHASE STEP TESTS
The following two tests are defined by the Standard in order to evaluate the dynamic behavior of an estimator during a transition between two steady states. The amplitude step test requires a sudden change in the amplitude of a signal at the nominal frequency. The change should amount to 10% transition up or down. Maximum response time t_r is among the more important parameters that needs to be evaluated in reference to the steady-state error limits. Formally, the response time is determined from the measured TVE as the difference between the time that TVE leaves the steady-state threshold accuracy and the time it returns to and remains within the next steady-state limit. Figure 12 shows the TVE during a time window between 1.8 and 2.2 s with the amplitude step occurring at the middle. The maximum TVE at approximately 5% is reached by all the estimators; however, the IPDFT reacts faster than the 3-cycle 3P and F3P, which is attributed to the use of non-rectangular window function. The shortest reaction time is achieved by switching to the 1-cycle F3P. Note that the IPDFT has no 1-cycle alternative. Table 2 lists the response times. Taking into account the maximum allowed time of $7/f_0 = 140$ ms, all the values are within the Standard requirements for the measurement class devices.

TABLE 2. Standard step test response times.

Algorithm	10% amplitude step [ms]	$\pi/18$ phase step [ms]
IPDFT [5]	22.9	26.6
3-cycle 3P [3]	48.0	53.8
3-cycle F3P	47.7	53.6
1-cycle F3P	19.1	19.5
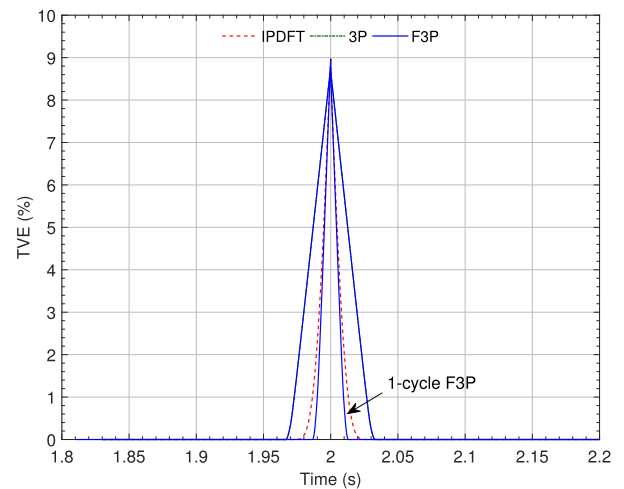
FIGURE 13. Phase step test; a $\pi/18$ step in phase angle occurs in the middle of time axis for a signal at nominal frequency. Time dynamics of the TVE is shown for the 1-cycle F3P (blue and labeled) and 3-cycle IPDFT [5] (red), 3P [3] (green) and F3P (blue) estimators.

The phase step test requires a sudden $\pi/18$ change in the phase angle. Figure 13 presents the results, this time with the maximum achievable TVE at 9%. The same conclusions can be drawn as for the above amplitude step test. The respective response times are available in Table 2. The IPDFT results closely resemble those reported in [5]. The F3P response

TABLE 3. Step test response times of competing approaches.

Algorithm	-20% amplitude step [ms]	$\pi/12$ phase step [ms]
IPDFT [5]	29	29
3-cycle 3P [3]	55	56
3-cycle F3P	55	56
1-cycle F3P	23	21
TPF[1] [3]	24	21
6PM[1] [13]	44	47
WLS[1] [12]	38	53

[1] Values reported in [5]

TABLE 4. Maximum TVE of competing approaches.

Algorithm	Off-nominal offset test [%]	Modulation test [%]	Ramp test [%]
IPDFT [5]	3e-3	0.60	0.03
3-cycle 3P [3]	1e-2	2.23	0.52
3-cycle F3P	2e-6	2.22	0.20
1-cycle F3P	2e-6	0.34	0.02
TPF[1] [3]	8e-2	0.34	0.74
6PM[1] [13]	8e-2	0.25	0.44
WLS[1] [12]	9e-4	0.04	0.60

[1] Values reported in [5]

times show no significant deviations if a frequency tracker is employed with the maximum FE in compliance with the Standard P-class threshold of ± 0.005 Hz.

D. COMPARISON TO THE REPORTED PERFORMANCES

The tests presented here closely resemble conditions adopted by some other researchers to allow for a credible comparison of the results. In addition to the IPDFT, 3P and the two F3P variants, Table 3 and Table 4 enlist results of the non-DFT based 6PM and WLS algorithms as well as that of the TPF, which is a single-cycle variant of the three-point filter. The values were reported by several papers, such as [25] and [26], and summarised in [5]. The 6PM is a six-parameter Taylor expansion estimator originally presented in [13], whereas the WLS computes phasors by postulating and solving a weighted least squares problem [12]. The response times for the amplitude step magnitude of -20% and the phase angle step magnitude of $\pi/12$ are shown in Table 3. Note that the steps are larger than those required by the Standard and presented in the previous subsection. Apart from the TPF, the 6PM and the WLS show response times slightly below the values reported for the 3-cycle F3P. Although designed for dynamic conditions, the 6PM and the WLS use a window of three and four cycles, respectively, which has some negative effect on the response times.

The maximum TVE values of the off-nominal offset tests in Table 4 are measured at 51 Hz. The F3P clearly stands out from the competing approaches. With respect to the dynamic performance, the modulation test of the F3P shows weakness with the maximum TVE above 2%, but with comparable performance to the other estimators if shorter window is used. The F3P performance in the ramp test is good even

if measured under the maximum frequency deviation. Here, the IPDFT and the 1-cycle F3P show the best results.

The reported IPDFT TVE of 0.2% at the SNR of 40 dB [5] was confirmed versus the 0.15% of the 3-cycle F3P and 0.25% of the 1-cycle F3P. Similarly, the out-of-band interference tests at lower 5% magnitude of 57.5 Hz and 85 Hz interfering signals were checked. In the former case, the maximum TVE values of 4.6%, 3.5% and 4.8% were obtained for the IPDFT, the 3-cycle F3P and the 1-cycle F3P, respectively. In the latter case of 85 Hz, the maximum TVE values of 0.7%, 0.2% and 1.7% were calculated.

V. DISCUSSION

The F3P is basically solving an overdetermined system of linear equations in complex domain for unknown phasor X, i.e., a system consisting of (4) at three indices r. The equations are carefully spaced in time to eliminate the unknown X^* by a simple average. The single-bin DFT and the frequency estimate need to be computed beforehand, with the values at noninteger indices linearly interpolated from the values at the closest integer indices. Other methods can be used to approximate similar systems of various degrees of freedom in the presence of noise; however, the three-point spacing provides an elegant and, more importantly, straightforward approach of low computational complexity.

It appears that the formulation of (8) violates the causality principle by referring to the future index $r + kN/6$. This is usually not a problem for digital filters, where a short delay line introduces only a small time penalty, e.g., roughly 3.4 ms at 50 Hz rated frequency. The latency, i.e., the time delay from the occurrence of an event to the time it is reported, caused by the method itself due to the window length and the three-point spacing angle is small in comparison to other contributing factors. Data time stamping is required by the Standard to synchronize measurements in applications. When the time reference of a phasor is being at the middle of a 3-cycle window and including the three-point delay, the inherent latency is approximately equal to 33.4 ms. The algorithm processing time, including the time spent for digital filtering and at the communication interface point is the prevailing factor. The Standard sets an upper limit on the total latency. Longer latencies are allowed for the measurement applications, with the prescribed upper limit of $7/f_r$ or $7/f_0$, whichever is greater, where f_r stands for the reporting rate. In the case of 25 reports per second, the maximum allowed latency is 280 ms, which is significantly larger than the latency of the method itself.

A prototype synchrophasor measurement unit based on the F3P has been developed and validated within the FP7 SUNSEED project [27]. Low and mid voltage grids of Kromberk testbed operated by Elektro Primorska were equipped with the units. The measurements were complemented by those of smart meters at the user sites and successfully exploited in the Distribution Network State Estimation (DSSE) experiment. In addition to 37 fully functional PMUs, more than 600 commercially available smart meters were employed in order to provide the grid state estimation, including the state

of nodes with no measurements available. The theoretical findings about the influence of uncertain model parameters and inaccurate measurements on the DSSE are studied in [24] and confirmed in the real-world setup. However, the topic of state estimation is beyond the scope of this paper. The interested reader is referred to the project deliverables [28].

VI. CONCLUSION

This paper proposed a frequency-adaptive three-point averaging filter for the single-bin DFT to improve the accuracy of power system's phasor measurements in static conditions. The errors of a classical DFT-based algorithm are a consequence of the well-known spectral leakage in the DFT when the sampling rate is matched to the rated frequency while measured frequency is allowed to drift within a narrow band. The choice of the particular phasor estimator was driven by the algorithm's low complexity and fast response. The F3P takes advantage of an independent frequency tracker in order to compensate for the leakage errors, including the effect of negative frequency infiltration, without the need of data resampling. The proposed correction establishes the ideal three-point spacing for the removal of the oscillating component. The performance is largely independent of the actual frequency deviation, at least in the frequency range expected in power systems. We quantified the impact of sampling rate and demonstrated the estimator's performance in a suite of steady- and dynamic-state tests defined by the relevant Standard. The simulation results prove the algorithm's superior performance in off-nominal frequency tests with and without the noise, good out-of-band interference results and some weakness in the harmonic distortion test when compared to the reference IPDFT based on the maximum sidelobe decay window. Less attractive is the multicycle dynamic performance, which can be significantly improved by the use of a single-cycle observation window, an option that is unavailable for the reference IPDFT.

APPENDIX A

The analytical expression for a phasor estimate based on the plain single-bin DFT and three-point filtering (3P) at off-nominal frequency f while the sampling clock is being locked to the rated frequency f_0 follows from (4) and (5)

$$
\begin{aligned}
X_r^{3P} &= \frac{1}{3}(X'_{r-\frac{N}{6}} + X'_r + X'_{r+\frac{N}{6}}) \\
&= \frac{1}{3}PX \left(e^{j(\omega-\omega_0)(t-\frac{T_0}{6})} + e^{j(\omega-\omega_0)t} \right. \\
&\quad \left. + e^{j(\omega-\omega_0)(t+\frac{T_0}{6})} \right) \\
&\quad + \frac{1}{3}QX^* \left(e^{-j(\omega+\omega_0)(t-\frac{T_0}{6})} + e^{-j(\omega+\omega_0)t} \right. \\
&\quad \left. + e^{-j(\omega+\omega_0)(t+\frac{T_0}{6})} \right) \\
&= \frac{1}{3}PXe^{j(\omega-\omega_0)t} \left(e^{j(1-\frac{\omega}{\omega_0})\frac{\pi}{3}} + 1 + e^{-j(1-\frac{\omega}{\omega_0})\frac{\pi}{3}} \right) \\
&\quad + \frac{1}{3}QX^*e^{-j(\omega+\omega_0)t} \left(e^{j(1+\frac{\omega}{\omega_0})\frac{\pi}{3}} + 1 + e^{-j(1+\frac{\omega}{\omega_0})\frac{\pi}{3}} \right)
\end{aligned}
$$

$$
\begin{aligned}
&= PXe^{j(\omega-\omega_0)t} \left(\frac{1}{3} + \frac{2}{3}\cos\left((1-\frac{\omega}{\omega_0})\frac{\pi}{3}\right) \right) \\
&\quad + QX^*e^{-j(\omega+\omega_0)t} \left(\frac{1}{3} + \frac{2}{3}\cos\left((1+\frac{\omega}{\omega_0})\frac{\pi}{3}\right) \right) \quad (22)
\end{aligned}
$$

by using $r\Delta t = t$, $N\Delta t = T_0$ and $T_0 = 2\pi/\omega_0$. In order to evaluate X_r^{3P}, $N/6$ needs to be a whole number.

APPENDIX B

Applying the same substitutions as in Appendix A, a closed-form alternative to (4) for a DFT with the frequency-corrected three-point filter (F3P) is

$$
\begin{aligned}
X_r^{F3P} &= \frac{1}{3}(X'_{r-k\frac{N}{6}} + X'_r + X'_{r+k\frac{N}{6}}) \\
&= \frac{1}{3}PX \left(e^{j(\omega-\omega_0)(t-k\frac{T_0}{6})} + e^{j(\omega-\omega_0)t} \right. \\
&\quad \left. + e^{j(\omega-\omega_0)(t+k\frac{T_0}{6})} \right) \\
&\quad + \frac{1}{3}QX^* \left(e^{-j(\omega+\omega_0)(t-k\frac{T_0}{6})} + e^{-j(\omega+\omega_0)t} \right. \\
&\quad \left. + e^{-j(\omega+\omega_0)(t+k\frac{T_0}{6})} \right) \\
&= \frac{1}{3}PXe^{j(\omega-\omega_0)t} \left(e^{-j\frac{2\pi}{3}\frac{(\omega-\omega_0)}{(\omega+\omega_0)}} + 1 + e^{j\frac{2\pi}{3}\frac{(\omega-\omega_0)}{(\omega+\omega_0)}} \right) \\
&\quad + \frac{1}{3}QX^*e^{-j(\omega+\omega_0)t} \left(e^{j\frac{2\pi}{3}} + 1 + e^{-j\frac{2\pi}{3}} \right) \\
&= PXe^{j(\omega-\omega_0)t} \left(\frac{1}{3} + \frac{2}{3}\cos\left(\frac{2\pi}{3}\frac{(\omega-\omega_0)}{(\omega+\omega_0)}\right) \right). \quad (23)
\end{aligned}
$$

Because $kN/6$ is generally a real number, the F3P estimate comes close to the closed-form expression as the sampling rate tends to infinity.

REFERENCES

[1] M. Alizadeh, X. Li, Z. Wang, A. Scaglione, and R. Melton, "Demand-side management in the smart grid: Information processing for the power switch," *IEEE Signal Process. Mag.*, vol. 29, no. 5, pp. 55–67, Sep. 2012, doi: 10.1109/msp.2012.2192951.

[2] G. Andria, M. Savino, and A. Trotta, "Windows and interpolation algorithms to improve electrical measurement accuracy," *IEEE Trans. Instrum. Meas.*, vol. 38, no. 4, pp. 856–863, Aug. 1989, doi: 10.1109/19.31004.

[3] A. G. Phadke and J. S. Thorp, *Synchronized Phasor Measurements and Their Applications*. New York, NY, USA: Springer, 2008.

[4] *IEEE/IEC International Standard—Measuring Relays and Protection Equipment—Part 118-1: Synchrophasor for Power Systems—Measurements*, Standard IEC/IEEE 60255-118-1, Dec. 2018, pp. 1–78, doi: 10.1109/IEEESTD.2018.8577045.

[5] D. Belega and D. Petri, "Accuracy analysis of the multicycle synchrophasor estimator provided by the interpolated DFT algorithm," *IEEE Trans. Instrum. Meas.*, vol. 62, no. 5, pp. 942–953, May 2013, doi: 10.1109/tim.2012.2236777.

[6] D. Belega and D. Dallet, "Multifrequency signal analysis by interpolated DFT method with maximum sidelobe decay windows," *Measurement*, vol. 42, no. 3, pp. 420–426, Apr. 2009, doi: 10.1016/j.measurement.2008.08.006.

[7] T. S. Sidhu, X. Zhang, and V. Balamourougan, "A new half-cycle phasor estimation algorithm," *IEEE Trans. Power Del.*, vol. 20, no. 2, pp. 1299–1305, Apr. 2005, doi: 10.1109/tpwrd.2004.834677.

[8] A. G. Phadke, J. S. Thorp, and M. G. Adamiak, "A new measurement technique for tracking voltage phasors, local system frequency, and rate of change of frequency," *IEEE Power Eng. Rev.*, vol. PER-3, no. 5, p. 23, May 1983, doi: 10.1109/MPER.1983.5519136.

[9] J. Warichet, T. Sezi, and J.-C. Maun, "Considerations about synchropha-sors measurement in dynamic system conditions," *Int. J. Electr. Power Energy Syst.*, vol. 31, no. 9, pp. 452–464, Oct. 2009, doi: 10.1016/j.ijepes.2009.03.035.

[10] A. K. Pradhan, A. Routray, and D. Sethi, "Voltage phasor estimation using complex linear Kalman filter," in *Proc. 8th IEE Int. Conf. Develop. Power Syst. Protection*, vol. 1, 2004, pp. 24–27, doi: 10.1049/cp:20040054.

[11] M. S. Sachdev and M. Nagpal, "A recursive least error squares algorithm for power system relaying and measurement applications," *IEEE Trans. Power Del.*, vol. 6, no. 3, pp. 1008–1015, Jul. 1991, doi: 10.1109/61.85841.

[12] M. A. Platas-Garza and J. A. D. L. O. Serna, "Dynamic phasor and frequency estimates through maximally flat differentiators," *IEEE Trans. Instrum. Meas.*, vol. 59, no. 7, pp. 1803–1811, Jul. 2010, doi: 10.1109/tim.2009.2030921.

[13] W. Premerlani, B. Kasztenny, and M. Adamiak, "Development and imple-mentation of a synchrophasor estimator capable of measurements under dynamic conditions," *IEEE Trans. Power Del.*, vol. 23, no. 1, pp. 109–123, Jan. 2008, doi: 10.1109/tpwrd.2007.910982.

[14] C.-K. Wong, I.-T. Leong, C.-S. Lei, J.-T. Wu, and Y.-D. Ham, "A novel algorithm for phasor calculation based on wavelet analysis [power system analysis]," in *Proc. Power Eng. Soc. Summer Meeting. Conf.*, vol. 3, Jul. 2001, pp. 1500–1503, doi: 10.1109/pess.2001.970298.

[15] J. A. D. L. O. Serna, "Synchrophasor estimation using Prony's method," *IEEE Trans. Instrum. Meas.*, vol. 62, no. 8, pp. 2119–2128, Aug. 2013, doi: 10.1109/tim.2013.2265436.

[16] P. Banerjee and S. C. Srivastava, "A subspace-based dynamic phasor estimator for synchrophasor application," *IEEE Trans. Instrum. Meas.*, vol. 61, no. 9, pp. 2436–2445, Sep. 2012, doi: 10.1109/tim.2012.2190336.

[17] K. Duda, T. P. Zielinski, A. Bien, and S. H. Barczentewicz, "Harmonic phasor estimation with flat-top FIR filter," *IEEE Trans. Instrum. Meas.*, vol. 69, no. 5, pp. 2039–2047, May 2020, doi: 10.1109/tim.2019.2918370.

[18] C. Liguori, A. Paolillo, and A. Pignotti, "An intelligent FFT analyzer with harmonic interference effect correction and uncertainty evaluation," *IEEE Trans. Instrum. Meas.*, vol. 53, no. 4, pp. 1125–1131, Aug. 2004, doi: 10.1109/tim.2004.831473.

[19] D. Belega, D. Macii, and D. Petri, "Fast synchrophasor estimation by means of frequency-domain and time-domain algorithms," *IEEE Trans. Instrum. Meas.*, vol. 63, no. 2, pp. 388–401, Feb. 2014, doi: 10.1109/tim.2013.2279000.

[20] P. Romano and M. Paolone, "Enhanced interpolated-DFT for syn-chrophasor estimation in FPGAs: Theory, implementation, and validation of a PMU prototype," *IEEE Trans. Instrum. Meas.*, vol. 63, no. 12, pp. 2824–2836, Dec. 2014, doi: 10.1109/tim.2014.2321463.

[21] C. Narduzzi, M. Bertocco, G. Frigo, and G. Giorgi, "Fast-TFM—Multifrequency phasor measurement for distribution networks," *IEEE Trans. Instrum. Meas.*, vol. 67, no. 8, pp. 1825–1835, Aug. 2018, doi: 10.1109/tim.2018.2809080.

[22] A. Xue, F. Xu, J. Xu, J. H. Chow, H. You, and T. Bi, "Correction of phasor measurements independent of transmission line parameters," *IEEE Trans. Smart Grid*, vol. 11, no. 1, pp. 346–356, Jan. 2020, doi: 10.1109/tsg.2019.2921819.

[23] J. Zhao, J. Tan, L. Wu, L. Zhan, W. Yao, and Y. Liu, "Impact of the measurement errors on synchrophasor-based WAMS applications," *IEEE Access*, vol. 7, pp. 143960–143972, 2019, doi: 10.1109/access.2019.2945786.

[24] U. Kuhar, M. Pantos, G. Kosec, and A. Svigelj, "The impact of model and measurement uncertainties on a state estimation in three-phase distribu-tion networks," *IEEE Trans. Smart Grid*, vol. 10, no. 3, pp. 3301–3310, May 2019, doi: 10.1109/tsg.2018.2823398.

[25] P. Castello, C. Muscas, and P. A. Pegoraro, "Performance comparison of algorithms for synchrophasors measurements under dynamic conditions," in *Proc. IEEE Int. Workshop Appl. Meas. Power Syst. (AMPS)*, Sep. 2011, pp. 25–30, doi: 10.1109/amps.2011.6090351.

[26] P. Castello, M. Lixia, C. Muscas, and P. A. Pegoraro, "Impact of the model on the accuracy of synchrophasor measurement," *IEEE Trans. Instrum. Meas.*, vol. 61, no. 8, pp. 2179–2188, Aug. 2012, doi: 10.1109/tim.2012.2193699.

[27] J. J. Nielsen, H. Ganem, L. Jorguseski, K. Alic, M. Smolnikar, Z. Zhu, N. K. Pratas, M. Golinski, H. Zhang, U. Kuhar, Z. Fan, and A. Svigelj, "Secure real-time monitoring and management of smart distribution grid using shared cellular networks," *IEEE Wireless Commun.*, vol. 24, no. 2, pp. 10–17, Apr. 2017, doi: 10.1109/mwc.2017.1600252.

[28] SUNSEED. *Sustainable and Robust Networking for Smart Electric-ity Distribution—D5.3 Field Trial Measurement Reports*. FP7-ICT-2013-11. Accessed: Feb. 24, 2021. [Online]. Available: http://sunseed-fp7.eu/deliverables/

ROMAN NOVAK (Member, IEEE) received the M.Sc. and Ph.D. degrees in computer science from the University of Ljubljana, in 1995 and 1998, respectively. He has been a Researcher with the Department of Communication Systems, Jožef Stefan Institute, Ljubljana, Slovenia, since 1992. He has been an Assistant Professor with the Jožef Stefan International Postgraduate School, since 2007. He was a Visiting Scientist with the Joan-neum Research, Graz, Austria, and the Graz Uni-versity of Technology, in 2008. In his professional career, he has been involved in numerous projects in the field of design and development of computer and telecommunication systems. His research interests include signal processing and parallel algorithms to the more specific topics, such as radio frequency propagation modelling and signal measurement.

• • •